



Adaptive meshing strategies for nanophotonics using a posteriori error estimation

Downloaded from: <https://research.chalmers.se>, 2026-06-11 22:29 UTC

Citation for the original published paper (version of record):

Jonasson Svärdsby, A., Tassin, P. (2024). Adaptive meshing strategies for nanophotonics using a posteriori error estimation. *Optics Express*, 32(14): 24592-24602.
<http://dx.doi.org/10.1364/OE.523907>

N.B. When citing this work, cite the original published paper.



Adaptive meshing strategies for nanophotonics using a posteriori error estimation

ALBIN J. SVÄRDSBY  AND PHILIPPE TASSIN

Department of Physics, Chalmers University of Technology, SE-41296 Göteborg, Sweden

Abstract: As nanophotonic devices become increasingly complex, computer simulations of such devices are becoming ever more important. Unfortunately, computer simulations of nanophotonic devices are computationally expensive, especially if many simulations are necessary, e.g., when optimizing or inverse designing a device. Here we study adaptive mesh refinement for finite-element method simulations using an a posteriori error estimation method. We demonstrate that the use of adaptive meshing leads to faster convergence with lower memory footprint for complex three-dimensional nanophotonic structures. Nevertheless, one needs to be careful to avoid a mesh propagation effect for adaptive mesh refinement to be a successful strategy.

© 2024 Optica Publishing Group under the terms of the [Optica Open Access Publishing Agreement](#)

1. Introduction

Since first conceived by Courant in 1941 [1], the finite element method has been developed into a mature method for solving partial differential equations and it is extensively used to solve problems in physics, chemistry, and engineering. In nanophotonics, finite-element simulations are often used to simulate the optical response of resonant structures. With ever increasing complexity of nanophotonic devices, inverse design—the computer-aided selection of a device geometry with a desired optical response—is gaining traction. This requires a large number of successive simulations in gradient-descent optimization techniques [2–5] or an even larger number of independent simulations in data-driven inverse design using machine learning [6–8]. The training data needed to achieve desired performance in such inverse design methods often requires tens of thousands of samples [9–12], in line with the number of samples typically needed for training generative adversarial network models on images [13] and with the number of samples in the CIFAR dataset [14] used in the seminal paper on generative adversarial networks [15]. Performing such a large number of simulations is on the edge of the possible for realistic nanophotonic devices. Speeding up such simulations will therefore have a positive impact on the usability of inverse design methods in nanophotonics as well as allow for more accurate simulations and simulation of larger devices such as gradient-phase metasurfaces [16–18].

When performing finite-element simulations, it is imperative to verify that the solution has converged. This can be achieved in two distinct ways. In h-FEM, the mesh elements are successively refined, whereas in p-FEM the degree of the polynomial basis functions is successively increased [19]. Szabó and Babuška have shown that exponential convergence can be achieved by allowing refinement of both the mesh size and the order of the polynomial basis functions in a process designated as hp-FEM [20–22] and methods to optimally decide between h- and p-refinement have been studied [23]. Further insights to hp-adaptive FEM for Maxwell's equations are provided in Ref. [24]. Here we want to perform adaptive mesh refinement in a simulation package commonly used in the nanophotonics field, necessarily limiting us to h-FEM, for which we can expect polynomial convergence at best. For the adaptive refinement of the mesh elements to work, some form of error estimation is needed. A posteriori error estimation was first developed for mechanics [25–27] and a number of ways to achieve a posteriori error estimation for Maxwell's equations were developed starting with the work of Monke [28] and Beck *et al.* [29]. A good overview of adaptive error estimation for finite-element simulations for nanophotonics can be found in Ref. [30].

In this article, we will study adaptive mesh refinement for electromagnetics simulations in COMSOL [31], a popular finite-element package used in the nanophotonics field. Adaptive mesh refinement opens up the possibility to simulate bigger structures by means of more clever resource allocation where we ensure that sections in the geometry are not overly resolved with a too fine mesh, resulting in unnecessary degrees of freedom to solve for. Alternatively, it allows to speed up simulations by reducing the number of degrees of freedom, which is particularly helpful in optimization and inverse design of photonic structures. We will compare three adaptive mesh refinement techniques: one based on an a posteriori error calculation for the Maxwell equations [32,33], a second technique using the built-in calculation of the L2 norm error estimate [34], and we compare this with the benchmark of uniform mesh refinement. We will apply these three mesh refinement techniques to three different systems: a realistic 3D simulation of an optical metasurface, a simpler Fabry-Perot cavity, and a surface plasmon propagating on a 2D material. Through these comparisons, we present scenarios these adaptive techniques are suitable for.

2. Adaptive mesh refinement

We focus here on h-FEM, where we keep the polynomial degree of the vector elements constant. Convergence is achieved by refining the mesh. Calling the exact solution of the electric field \mathbf{E} and the FEM approximation \mathbf{E}_{FEM} , we seek the computational error

$$\mathbf{e} = \mathbf{E} - \mathbf{E}_{\text{FEM}}. \quad (1)$$

If we integrate the norm of the error over each mesh cell, we get the relative contribution of each mesh cell to the error of the finite-element solution, which we can then use to determine the mesh cell refinement.

The method of adaptive mesh refinement we will use is based on the a posteriori error estimation method developed by Izsak *et al.* [33], building on earlier work by Ainsworth and Oden [32]. This method uses an a posteriori calculation of the computational error \mathbf{e} , i.e., after having performed an initial FEM simulation.

We construct the following bilinear form over a mesh cell K

$$B_K(\mathbf{e}, \mathbf{v}) \equiv [(\nabla \times \mathbf{e}) \cdot (\nabla \times \mathbf{v})] - k^2(\mathbf{e} \cdot \mathbf{v}), \quad (2)$$

where the subscript K indicates integration over the mesh cell, \mathbf{v} is an arbitrary vector field, and k is the local wavenumber. Expanding the error \mathbf{e} using Eq. (1) yields

$$B_K(\mathbf{e}, \mathbf{v}) = (\nabla \times \mathbf{E}) \cdot (\nabla \times \mathbf{v}) - k^2(\mathbf{E} \cdot \mathbf{v}) - (\nabla \times \mathbf{E}_{\text{FEM}}) \cdot (\nabla \times \mathbf{v}) + k^2(\mathbf{E}_{\text{FEM}} \cdot \mathbf{v}). \quad (3)$$

Partial integration of Eq. (3) gives

$$B_K(\mathbf{e}, \mathbf{v}) = [(\nabla \times \nabla \times \mathbf{E}) \cdot \mathbf{v} - k^2(\mathbf{E} \cdot \mathbf{v}) - B_K(\mathbf{E}_{\text{FEM}} \cdot \mathbf{v})]_K + [(\mathbf{n} \times (\nabla \times \mathbf{E})) \cdot (\mathbf{n} \times (\mathbf{n} \times \mathbf{v}))]_{\partial K}, \quad (4)$$

where $[\]_K$ and $[\]_{\partial K}$ denote integration over the domain K and its boundary, ∂K , respectively. The bilinear form in Eq. (4) can be simplified by writing it in terms of the current density, \mathbf{J} , which is

known:

$$B_K(\mathbf{e}, \mathbf{v}) = [\mathbf{J} \cdot \mathbf{v} - B_K(\mathbf{E}_{\text{FEM}} \cdot \mathbf{v})]_K + [(\mathbf{n} \times (\nabla \times \mathbf{E})) \cdot (\mathbf{n} \times (\mathbf{n} \times \mathbf{v}))]_{\partial K}. \quad (5)$$

Since we do not know the exact solution, we have to approximate $\nabla \times \mathbf{E}$ by the average of the tangential traces on each side of the mesh element boundary ∂K [33], as illustrated in Fig. 1:

$$[\mathbf{n} \times (\nabla \times \mathbf{E})]_{\partial K} \approx \frac{1}{2} \mathbf{n} \times (\nabla \times \mathbf{E}_{\text{FEM, up}} + \nabla \times \mathbf{E}_{\text{FEM, down}}). \quad (6)$$

For this approximation to work, bubble functions are used as shape functions for the calculation of the computational error [32].

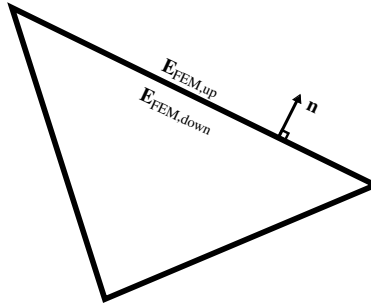


Fig. 1. Schematic illustration of a mesh element with the tangential traces of the electric field.

Solving Eq. (5), we get the error \mathbf{e} . To obtain a scalar measure for the error, we need to take the norm of \mathbf{e} . The norm on a Banach space can be chosen in different ways and can also include derivatives. Following Ref. [33], we choose the curl norm, but we add a correction term in front of the curl term to ensure correct dimensions. This results in the final error:

$$\|\mathbf{e}\|_{\text{curl},K} = \left(\|\mathbf{e}\|^2 + \left(\frac{c_0}{2\pi\sqrt{\epsilon_{rf}}} \right)^2 \|\nabla \times \mathbf{e}\|^2 \right)^{1/2}. \quad (7)$$

We can now identify the first term as the error on the electric field and the second term as the error on the magnetic field, since $\nabla \times \mathbf{e} = \nabla \times \mathbf{E} - \nabla \times \mathbf{E}_{\text{FEM}} \propto \mathbf{B} - \mathbf{B}_{\text{FEM}}$. The choice of the curl norm therefore ensures that the electromagnetic energy is resolved, irrespective of whether the energy is stored in the electric or the magnetic field.

3. Adaptive meshing of a Fabry-Perot cavity

In the remainder of this article, we will assess the a posteriori meshing method and use it for adaptive meshing of 3D structures. We start with a rather simple Fabry-Perot cavity, for which we know that it exhibits complete transmission if the frequency of the incident light is tuned to one of the resonance frequencies. The geometry is shown in Fig. 2, where the middle section is made of a material with a large index of refraction. At resonance, a large electric field is built up in the middle section. We simulate the transmission of light through the cavity by allowing a plane wave to travel perpendicular to the material interface. The simulations are performed using COMSOL Multiphysics [31], in which we also implement the a posteriori error calculation.

We will compare the adaptive meshing using the following three meshing methods:

- **Uniform meshing:** the maximum element size is determined by the wavelength divided by the refractive index and multiplied with a swept scaling factor: $\lambda/n * r_s$;

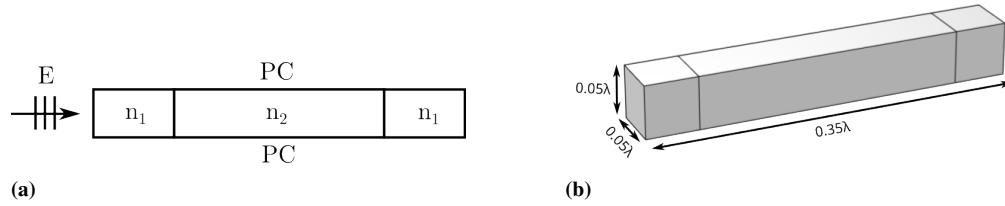


Fig. 2. A Fabry-Perot cavity with a dielectric slab in the middle and air to the left and the right. The length of the middle section is tuned so we excite a resonance and achieve total transmission. (a) shows the schematic dimensions of the cavity where the plane wave is exciting it from the left, with periodic boundary conditions perpendicular to the propagation direction, whereas (b) shows the full 3D structure. The indices of refraction used are $n_1 = 1$ and $n_2 = 2$.

- **A posteriori meshing:** the mesh is refined based on the computational error of each mesh element using the method described in Sec. 2;
- **L2 meshing:** the mesh is refined using the L2 norm of the field [31]. The L2 indicator used over domain K and area A is

$$e_{L2, \text{norm}} = \left(\int_K \sum_l s_l^{-2} h^{2q_l} |p_l|^2 dA \right)^{1/2}, \quad (8)$$

where s_l is a scaling factor (here $s_l = 1$), p_l is the residual in the l :th equation, q_l is the stability estimate derivative order (here $q_l = 2$), and h is the local mesh element size. The local error indicator for the mesh element used is

$$e_{\text{element}} = \sum_l s_l^{-2} h^{2q_l} |\tau_l|^2 A, \quad (9)$$

where A is the size of the mesh element (volume in 3D, area in 2D, length in 1D), and τ_l is the l :th residual for each element.

In order to achieve a fair comparison, we tune the three mesh refinement methods so that each method increases with approximately the same number of mesh elements for a given iteration. This is reflected in Fig. 3(a), where we plot the degrees of freedom of the finite-element model for successive iterations of the mesh refinement.

We then plot the calculated transmission as a function of the degrees of freedom of the model in Fig. 3(b). We observe that all refinement methods converge to the exact solution. Upon closer inspection (see Figs. 3(c) and 3(d)), we see that uniform mesh refinement converges faster initially, but the refinement method based on the a posteriori error estimation overtakes the uniform refinement method for smaller mesh sizes. This is not entirely surprising, since the field is uniform in the middle section of the Fabry-Perot cavity and uniform refinement is therefore quite effective for the Fabry-Perot cavity problem. At later iterations, the space before and after the Fabry-Perot resonator, with smaller index of refraction, gets meshed too dense, and the smarter adaptive mesh refinement methods can overtake the uniform mesh refinement.

Finally, we compare the total wall-clock time for the three mesh refinement methods in Fig. 3(e) and 3(f). We observe that all three methods take roughly the same time to converge, with a small advantage for the L2 mesh refinement method for finer resolutions. We note that this is not surprising, since uniform mesh refinement provides a mesh that correlates with the energy density for the Fabry-Perot cavity.

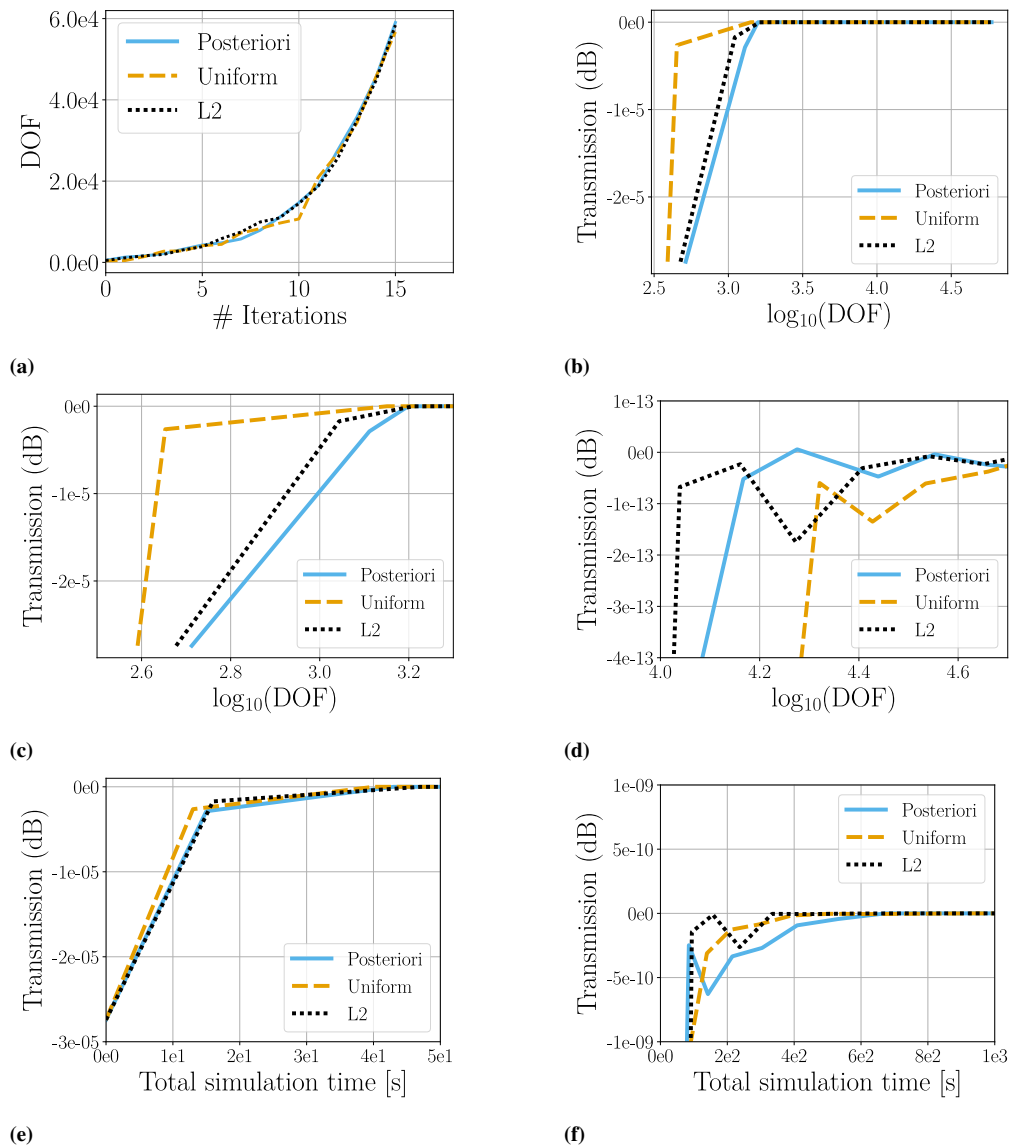


Fig. 3. Comparison of the performance of the three mesh refinement methods for a Fabry-Perot cavity. (a) shows the degrees of freedom vs. iteration steps in the refinement. (b) shows the transmission amplitude of the Fabry-Perot cavity as a function of degrees of freedom. (c) and (d) are zoomed-in versions containing the beginning and end, respectively, and (e) and (f) show the transmission as a function of the total simulation time.

4. Adaptive mesh refinement of a complex meta-atom

Having investigated the geometry of the Fabry-Perot cavity in Sec. 3, we now move to a nanophotonic structure with stronger field localization and more complicated geometry. The system we consider here is a periodic metasurface illuminated by a plane monochromatic wave. The unit cell of the metasurface is shown in Fig. 4(a) and was created by a machine-learning-based inverse design method [9].

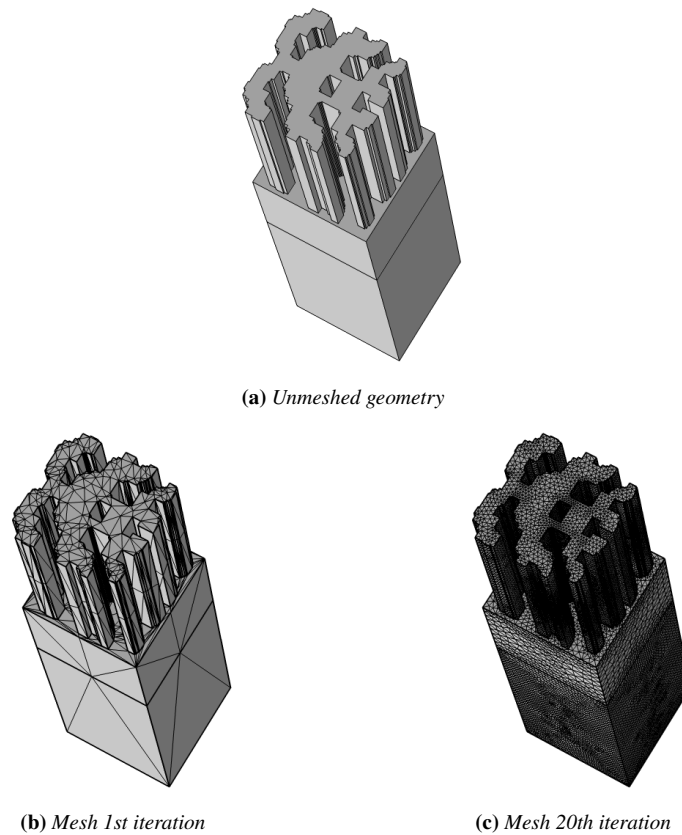


Fig. 4. Meta-atom consisting of different materials to showcase a scenario with complex geometry, in the form of a metasurface. (a)–(c) show different iterations of mesh refinement. The length of the quadratic base is 0.38λ and the minimum feature size of the geometry has a length of 0.02λ .

The meshes at two different iterations are shown in Fig. 4. We observe that the mesh adaptation refines regions with smaller geometries and higher refractive indices (the substrate and the patterned layer). As before, we tuned the methods so that the three methods increase the degrees of freedom at the same rate (see Fig. 5(a)).

From Figs. 5(b)–5(d), we can see that the two adaptive mesh refinement methods converge faster than the uniform refinement method in terms of degrees of freedom. Out of the two adaptive methods described in this paper, L2 and a posteriori perform similarly, with a slight initial advantage for the a posteriori mesh refinement method. This is in line with what can be expected, since the method based on a posteriori error estimation calculates the error from Maxwell's equations, while the L2-norm method can only compare the change in the fields

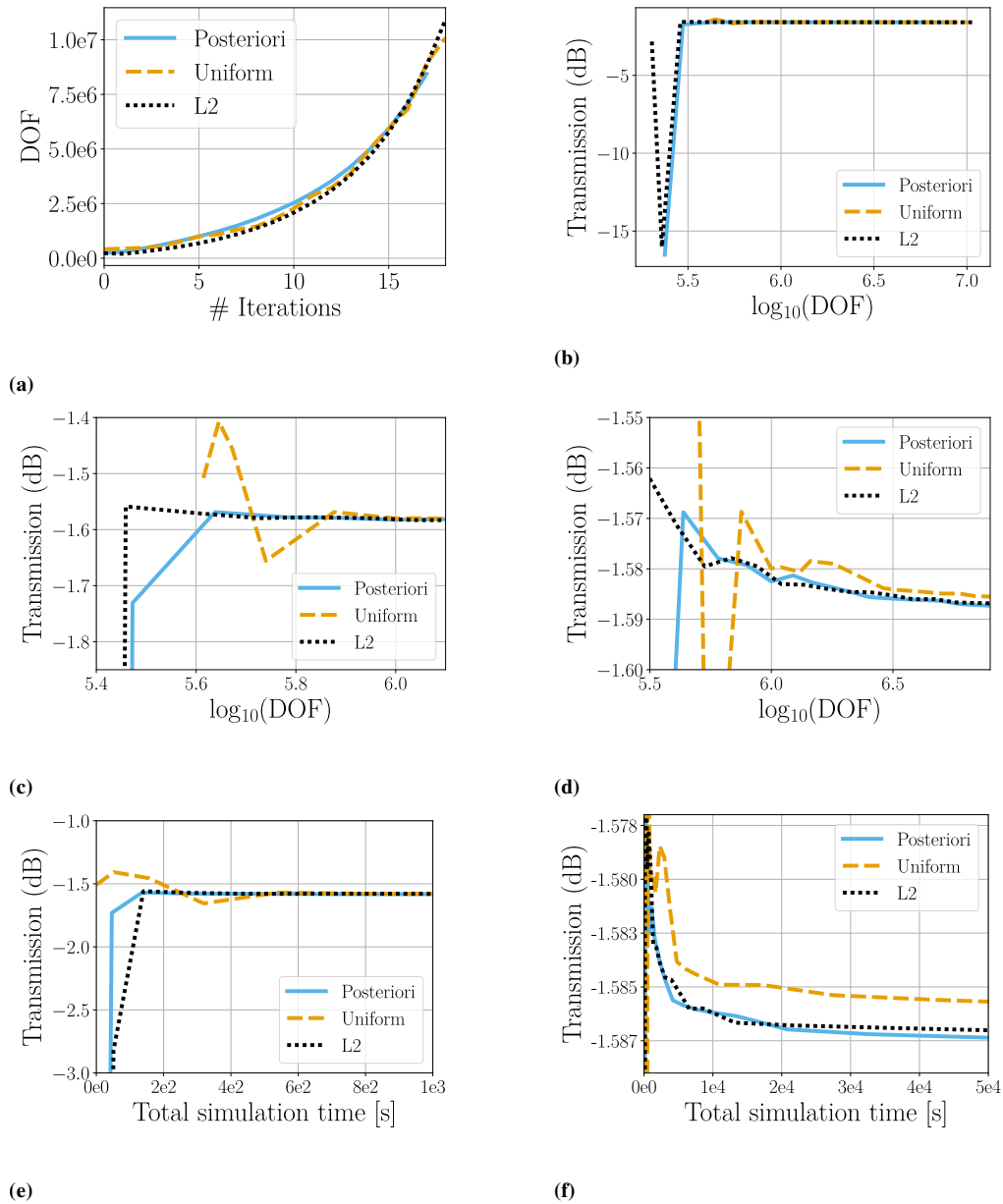


Fig. 5. Comparison of the performance of the three mesh refinement methods for a metasurface with complex geometry. (a) shows the degrees of freedom as a function of iteration step, in the refinement. (b) shows the transmission amplitude of the Fabry-Perot cavity as a function of degrees of freedom. (c) and (d) are zoomed-in versions containing the beginning and end, respectively. (e) and (f) show the transmission as a function of the total simulation time.

between iterations. The method based on a posteriori error estimation has, therefore, better guidance for its mesh refinement in structures with localized electromagnetic fields.

Comparing the total simulation time in Figs. 5(e)–5(f), we observe that the traditional uniform mesh refinement approach is quicker initially, but is then overtaken by the adaptive methods when approaching finer mesh resolutions. The two adaptive methods perform similarly with a slight advantage for the method with a posteriori error estimation for longer and higher-resolution simulations.

5. Mesh propagation effect

Finally, we want to understand how the a posteriori mesh refinement method behaves under more extreme circumstances. To that purpose, we simulate a surface plasmon propagating over the 2D material black phosphorous. Such plasmons are extremely well confined to the 2D material surface and need therefore a very fine mesh in a few nanometers' distance from the surface to capture the exponential decay of the electromagnetic fields away from the surface.

The mesh for different iterations of the a posteriori mesh refinement procedure is shown in Figs. 6 and 7 for the scenario where an incoming plane surface plasmon is injected from the left using a boundary condition. Starting from a reasonably fine mesh, as seen in Fig. 6(a), the mesh is then refined in a narrow volume close to the 2D material surface, creating a better resolution where the fields are strongest. A uniform mesh strategy would perform much worse here as it would mesh the space above and below the surface equally fine, leading to extremely large models. It is in these scenarios with very strong field confinement that the mesh refinement based on the a posteriori error estimation is most useful.

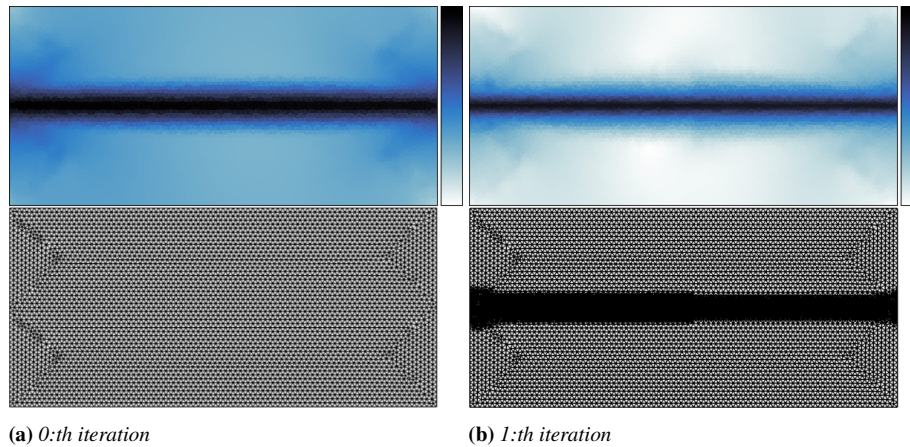


Fig. 6. Mesh progression starting from a finer mesh. A horizontal surface charge is present in the middle of the structure. Note that mesh refinement occurs along the entire surface charge. The top part of each panel shows the mesh element error in logarithmic scale and the bottom figures show the actual mesh.

However, when we start the same simulation from a much coarser mesh as seen Fig. 7(a) and observe how the mesh is refined at the different iteration steps, detailed in Fig. 7, the plasmon wave does initially not propagate all the way to the right in the discretized model until the mesh has been sufficiently refined. In this scenario, strong local fields are created near the left-most boundary, which results in mesh refinement only close to the left-most boundary. This, then, hinders the surface plasmon to propagate to the right as it should. This leads us to the conclusion that we cannot start from a too coarse mesh when using the adaptive mesh refinement method based on a posteriori error estimation.

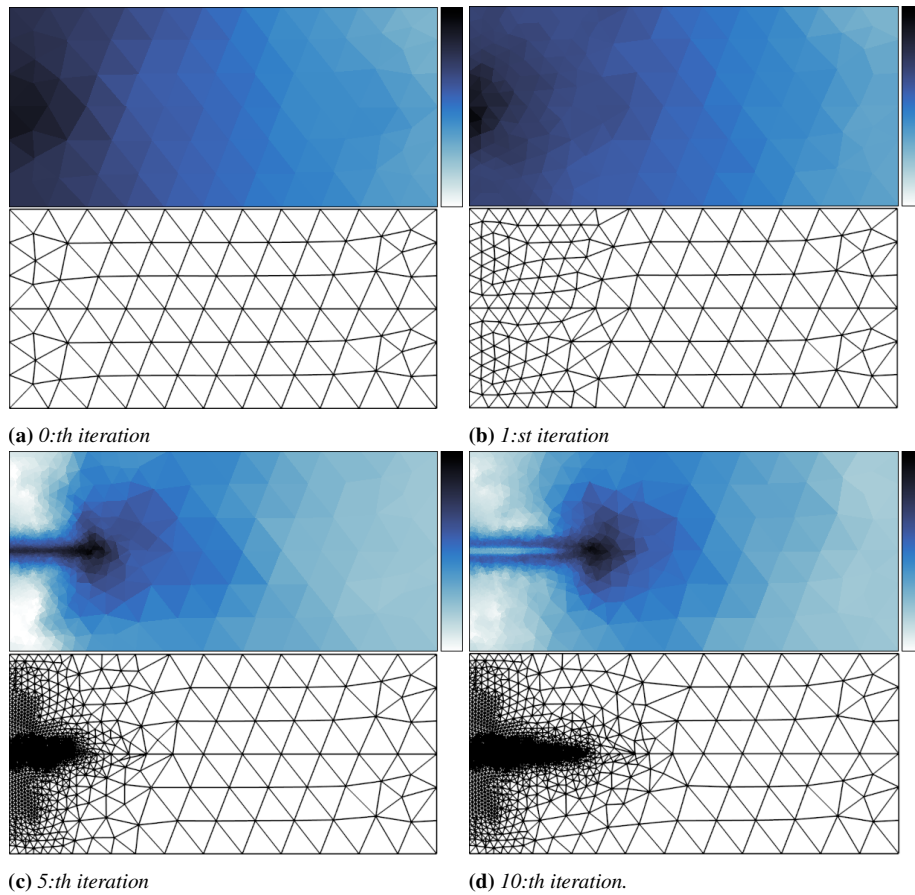


Fig. 7. Mesh progression starting from a very coarse mesh. A horizontal surface charge is present in the middle of the structure. The mesh is not fine enough to propagate the plasmon to the right, so the refinement gets stuck in the early iterations. The top part of each panel shows the mesh element error in logarithmic scale and the bottom figures show the actual mesh.

6. Conclusions

We have compared three mesh refinement methods for finite-element simulations in nanophotonics. From our results, we conclude that mesh refinement based on a posteriori error estimation can reduce the number of degrees of freedom and the total wall-clock time for the simulation of nanophotonic devices, especially for devices with complex geometry or devices with strong field localization. For simulations with smaller and less complex geometries, mesh refinement based on the L2 norm may be a good alternative, as it is easier to implement (no additional finite-element simulations for the error estimation is needed) and its performance is similar in terms of memory usage, and only moderately slower in terms of wall-clock time. When the energy density distribution is quasi-uniform, i.e., when no considerable light localization takes place, uniform mesh refinement can be used. These conclusions and recommendations for different use cases of adaptive meshing are also presented in Table 1. One must be careful, however, not to start with a too coarse mesh when using mesh refinement based on a posteriori error estimation, as this can lead to a mesh propagation effect that substantially slows down the convergence of the mesh refinement process.

Table 1. Table showing a recommendation of when to use different meshing techniques.

Meshing method	Result	Suitable scenario
A posteriori	Fastest, lowest number of DOFs	Complex and resonant geometries with strong light localization
L2	Slightly slower than with a posteriori error estimation	Smaller models with light localization
Uniform	Slowest	Devices with quasi-uniform energy distribution

We believe that use of automatic mesh refinement may allow to solve problems in nanophotonics that currently cannot be solved on state-of-the-art computing infrastructure. It may also be used in conjunction with the beam envelope method applied to larger optical devices, where the mesh cells can be much larger except in points with strong reflections or strong field localization, where a solution of Maxwell's equations on the subwavelength scale is required. Here, very nonuniform meshes created by a mesh refinement may be very useful. Finally, our approach can also be used in the area of nonlinear optics, where field enhancement is often desired. Since the a posteriori error estimation does not require solving large equation systems, the additional overhead one would get in the simulation of nonlinear optical devices caused by the error estimation may be negligible.

Funding. Vetenskapsrådet.

Acknowledgments. We acknowledge partial financial support from the Swedish Research Council under Grant No. 2020-05284. Simulations were performed on resources provided by the Swedish National Infrastructure for Computing (NAISS), at the Chalmers/C3SE site, partially funded by the Swedish Research Council under Grant No. 2022-06725. The work was partially performed in the framework of the Excellence Center META-PIX.

Disclosures. The authors declare no conflicts of interest.

Data availability. Data underlying the results presented in this paper are not publicly available at this time but may be obtained from the authors upon reasonable request.

References

1. R. Courant, "Variational methods for the solution of problems of equilibrium and vibrations," *Bull. Am. Math.* **49**(1), 1–23 (1943).
2. Y. Elesin, B. S. Lazarov, J. S. Jensen, *et al.*, "Design of robust and efficient photonic switches using topology optimization," *Photonics Nanostruct. Fundam. Appl.* **10**(1), 153–165 (2012).
3. C. M. Lalau-Keraly, S. Bhargava, O. D. Miller, *et al.*, "Adjoint shape optimization applied to electromagnetic design," *Opt. Express* **21**(18), 21693–21701 (2013).
4. A. Y. Pigott, J. Lu, K. G. Lagoudakis, *et al.*, "Inverse design and demonstration of a compact and broadband on-chip wavelength demultiplexer," *Nat. Photonics* **9**(6), 374–377 (2015).
5. L. Beilina, L. Mpinganzima, and P. Tassin, "Adaptive optimization algorithm for the computational design of nanophotonic structures," in *International Conference on Electromagnetics in Advanced Applications* (IEEE, 2016), pp. 420–423.
6. J. Peurifoy, Y. Shen, L. Jing, *et al.*, "Nanophotonic particle simulation and inverse design using artificial neural networks," *Sci. Adv.* **4**(6), eaar4206 (2018).
7. D. Liu, Y. Tan, E. Khoram, *et al.*, "Training deep neural networks for the inverse design of nanophotonic structures," *ACS Photonics* **5**(4), 1365–1369 (2018).
8. E. S. Harper, E. J. Coyle, J. P. Vernon, *et al.*, "Inverse design of broadband highly reflective metasurfaces using neural networks," *Phys. Rev. B* **101**(19), 195104 (2020).
9. T. Gahlmann and P. Tassin, "Deep neural networks for the prediction of the optical properties and the free-form inverse design of metamaterials," *Phys. Rev. B* **106**(8), 085408 (2022).
10. R. S. Hegde, "Photonics inverse design: Pairing deep neural networks with evolutionary algorithms," *IEEE J. Sel. Top. Quantum Electron.* **26**(1), 1–8 (2020).
11. W. Ma, F. Cheng, and Y. Liu, "Deep-Learning-Enabled On-Demand Design of Chiral Metamaterials," *ACS Nano* **12**(6), 6326–6334 (2018).
12. S. So, T. Badloe, J. Noh, *et al.*, "Deep learning enabled inverse design in nanophotonics," *Nanophotonics* **9**(5), 1041–1057 (2020).

13. T. Karras, M. Aittala, J. Hellsten, *et al.*, “Training Generative Adversarial Networks with Limited Data,” in *Advances in Neural Information Processing Systems*, vol. 33 H. Larochelle, M. Ranzato, R. Hadsell, *et al.*, eds. (Curran Associates, Inc., 2020), pp. 12104–12114.
14. A. Krizhevsky and G. Hinton, *Learning Multiple Layers of Features from Tiny Images* (University of Toronto, 2009).
15. I. Goodfellow, J. Pouget-Abadie, M. Mirza, *et al.*, “Generative adversarial nets,” *Adv. Neural Inf. Process. Syst.* **27**, 2672–2680 (2014).
16. G. Zheng, H. Mühlenbernd, M. Kenney, *et al.*, “Metasurface holograms reaching 80% efficiency,” *Nat. Nanotechnol.* **10**(4), 308–312 (2015).
17. A. Arbabi, E. Arbabi, Y. Horie, *et al.*, “Planar metasurface retroreflector,” *Nat. Photonics* **11**(7), 415–420 (2017).
18. P. Genevet, F. Capasso, F. Aieta, *et al.*, “Recent advances in planar optics: From plasmonic to dielectric metasurfaces,” *Optica* **4**(1), 139–152 (2017).
19. B. A. Szabo and A. K. Mehta, “p-convergent finite element approximations in fracture mechanics,” *Int. J. Numer. Methods Eng.* **12**(3), 551–560 (1978).
20. I. Babuska and B. A. Szabo, “On the rates of convergence of the finite element method,” *Int. J. Numer. Methods Eng.* **18**(3), 323–341 (1982).
21. I. Babuska, B. A. Szabo, and I. N. Katz, “The p-version of the finite element method,” *SIAM J. Numer. Anal.* **18**(3), 515–545 (1981).
22. I. Babuška, “The p and h-p versions of the Finite Element Method: The State of the Art,” in *Finite Elements*, D. L. Dwoyer, M. Y. Hussaini, and R. G. Voigt, eds. (Springer, 1988), pp. 199–239.
23. W. F. Mitchell and M. A. McClain, “A Comparison of hp-Adaptive Strategies for Elliptic Partial Differential Equations,” *ACM Trans. Math. Softw.* **41**(1), 1–39 (2014).
24. L. Demkowicz, J. Kurtz, D. Pardo, *et al.*, *Computing with Hp-Adaptive Finite Elements, Vol. 2: Frontiers Three Dimensional Elliptic and Maxwell Problems with Applications* (Chapman & Hall/CRC, 2007), 1st ed.
25. M. Paraschivou, J. Peraire, and A. T. Patera, “A posteriori finite element bounds for linear-functional outputs of elliptic partial differential equations,” *Comput. Methods Appl. Mech. Eng.* **150**(1–4), 289–312 (1997).
26. R. Becker and R. Rannacher, *Weighted A Posteriori Error Control in FE Methods* (Universität Heidelberg, 1997).
27. J. T. Oden and S. Prudhomme, “Goal-oriented error estimation and adaptivity for the finite element method,” *Comput. Math. with Appl.* **41**(5–6), 735–756 (2001).
28. P. Monk, “A posteriori error indicators for Maxwell’s equations,” *J. Comput. Appl.* **100**(2), 173–190 (1998).
29. R. Beck, R. Hiptmair, R. H. W. Hoppe, *et al.*, “Residual based a posteriori error estimators for eddy current computation,” *ESAIM Math Model. Numer.* **34**(1), 159–182 (2000).
30. J. Li and Y. Huang, *Time-Domain Finite Element Methods for Maxwell’s Equations in Metamaterials* (Springer, 2013).
31. “COMSOL Multiphysics” (2022).
32. M. Ainsworth and J. T. Oden, “A posteriori error estimation in finite element analysis,” *Comput. Methods Appl. Mech. Eng.* **142**(1–2), 1–88 (1997).
33. F. Izsák, D. Harutyunyan, and J. J. W. Van Der Vegt, “Implicit a posteriori error estimates for the Maxwell equations,” *Math. Comput.* **77**(263), 1355–1386 (2008).
34. R. Verfurth, *A Review of Posteriori Error Estimation & Adaptive Mesh-Refinement Techniques* (Wiley, 1996).